ACS MATERIALS LETTERS
www.acsmaterialsletters.org
Letter

Finding the First Squarates Nonlinear Optical Crystal $NaHC_4O_4{\cdot}H_2O$ with Strong Second Harmonic Generation and Giant Birefringence

Xiaodong Zhang, Dongxu Cao, Daqing Yang, Ying Wang, Kui Wu, Ming-Hsien Lee, and Bingbing Zhang*

Cite This: ACS Materials Lett. 2022, 4, 572–576
Read Online

ABSTRACT: **With the development of laser technology, nonlinear optical (NLO) crystals with optimal performance are urgently required. Finding new NLO-active units is necessary to expand the exploration systems for NLO materials. Herein, a π-conjugated planar hydrogensquarate $(HC_4O_4)^-$ with large hyperpolarizabilities and giant polarizability anisotropies is identified as a new NLO-active unit. On the basis of this idea, a new NLO crystal $NaHC_4O_4{\cdot}H_2O$ is found by using the first-principles high-throughput screening pipeline for nonlinear optical materials (FHSP-NLO). It is the first NLO crystal found in squarates. Subsequently, the crystal with a size of 30 × 6 × 5 mm was grown by a facile aqueous solution method. $NaHC_4O_4{\cdot}H_2O$ shows a strong powder SHG effect of 2.3 × KDP and a giant birefringence of 0.52 at 1064 nm. Electronic structure calculation and analysis reveal that the π orbitals of the $(HC_4O_4)^-$ groups are the dominant source of the SHG coefficient. This study provides novel NLO-active units and a materials system to design and find NLO crystals.**

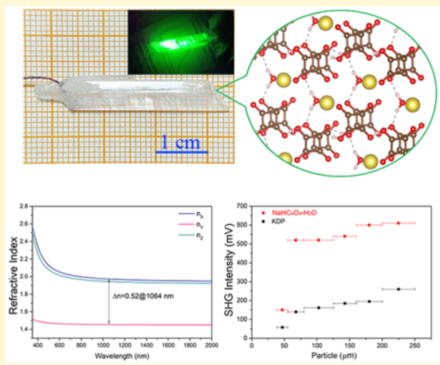

Nonlinear optical (NLO) crystals are the key materials to convert the frequency of coherent lasers that are widely used in a variety of applications including spectroscopy, communication, generation of entangled photon pairs, environmental monitoring spectroscopy, and detection of explosives.[1−8] The searching of NLO crystals was mainly concentrated in systems containing NLO-active units such as π-conjugated planar units ($(BO_3)^{3-}$, $(CO_3)^{2-}$, $(NO_3)^-$), and cations susceptible to second-order Jahn−Teller effect (SOJTE) distortions, including d^0 transition metals cations and stereoactive lone-pairs cations.[9−12] Over the past 60 years, many NLO materials have been found in corresponding materials' systems including $LiNbO_3$ (LN),[13] KIO_3,[14] β-BaB_2O_4 (BBO),[15] LiB_3O_5 (LBO),[16] and $KBe_2BO_3F_2$ (KBBF).[17] With the development of laser technology, NLO crystals with optimal performance are urgently required. However, it is more and more difficult to find a new NLO crystal that is better than existing materials in traditional systems.

To break through the stagnant situation, finding new NLO-active units is necessary to expand the exploration systems for NLO materials. Recently, some new NLO-active units are proposed and promote a new wave of research for NLO crystals. For example, $[BO_xF_{4-x}]$(x = 1,2,3) units could optimize the mutually restricted properties and have created a new field for finding deep-ultraviolet (DUV) NLO crystals. Subsequently, some structural groups including $(PO_3F)^{2-}$, $(PO_2F_2)^-$, $(C_3N_3O_3)^{3-}$, $[C(NH_2)_3]^+$, $(BS_3)^{3-}$, $(SiN_xO_{4-x})^{(x+4)-}$ (x = 1, 2, 3) are proposed as new NLO-active units. Many new NLO materials with good properties have been found and identified such as $(NH_4)_2PO_3F$,[18,19] $Ca_3(C_3N_3O_3)_2$,[20] $KLiHC_3N_3O_3{\cdot}2H_2O$,[21] $C(NH_2)_3SO_3F$,[22] $[C(NH_2)_3]_6(PO_4)_2{\cdot}3H_2O$,[23] BaB_2S_4,[24] and LiSiON.[25] These units could be classified into two categories: π-conjugated planar units and non-π-conjugated heteroleptic tetrahedral. Among them, π-conjugated planar units show large hyperpolarizabilities and polarizability anisotropies. They are essential to NLO and birefringent materials to induce a strong SHG response and large birefringence.

Carbon atoms with sp^2 hybridized orbitals bonded with oxygen atoms forming NLO-active planar $(CO_3)^{2-}$ units. In addition, C and O atoms could form diverse π-conjugated

Received: February 7, 2022
Accepted: February 24, 2022
Published: March 2, 2022

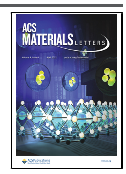

planar oxocarbon anions including $(C_2O_4)^{2-}$, $(C_2O_6)^{2-}$, $(C_4O_4)^{2-}$, and $(C_6O_6)^{2-}$. All of them shown large polarizability anisotropies and are proposed as novel birefringence-active units.[26] Unfortunately, these oxocarbon anions are centrosymmetric and have no microscopic second-order susceptibility. The "anionic group theory" suggests that the macroscopic SHG coefficients of crystals originate from a geometrical superposition of the microscopic second-order susceptibility. Accordingly, these oxocarbon anions with centrosymmetric structure are excluded from NLO-active units. Besides, most of the crystals that contain these anions are centrosymmetric. Only $(NH_4)_2C_2O_4{\cdot}H_2O$, which is crystallized in a noncentrosymmetric structure, shows a large birefringence of 0.1587 at 546 nm[27] but a relatively small SHG coefficient.[28]

In this work, we find a new NLO-active π-conjugated planar anionic group $(HC_4O_4)^-$. Hydrogenating the $(C_4O_4)^{2-}$ anionic group could break its centrosymmetry, induce large hyperpolarizabilities, and retain giant polarizability anisotropies. To investigate the NLO-related properties of $(C_4O_4)^{2-}$ and $(HC_4O_4)^-$ anionic groups as well as the $H_2C_4O_4$ molecule (represented by $(H_xC_4O_4)^{(2-x)-}$, $x = 0, 1, 2$), their electronic structure, HOMO−LUMO gap, polarizability, and hyperpolarizability are calculated using density functional theory (DFT) method implemented by the Gaussian09[29] package at the B3LYP/6-31G level. For comparison, the same properties of $(CO_3)^{2-}$ are also calculated. As listed in Table S1 and shown in Figure 1, $(C_4O_4)^{2-}$, $(HC_4O_4)^-$, and $H_2C_4O_4$ show an

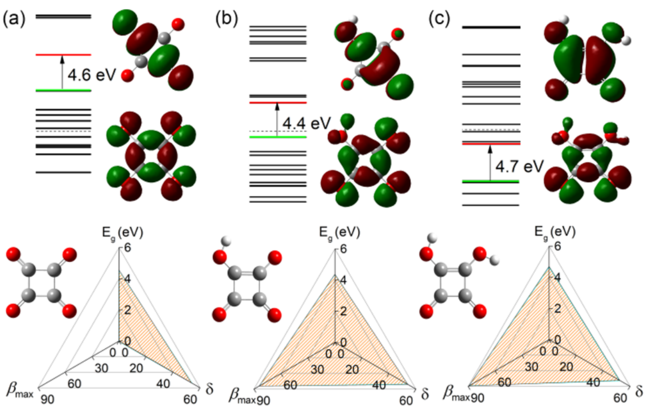

Figure 1. Electronic energy-level, HOMO and LUMO orbitals, radar chart of polarizability anisotropy (δ), maximum hyperpolarizability tensor (β_{max}), HOMO−LUMO gap (E_g) of (a) (C4O4)$^{2-}$, (b) $(HC_4O_4)^-$, and (c) $H_2C_4O_4$.

energy gap between 4.4 and 4.7 eV. The $(C_4O_4)^{2-}$, $(HC_4O_4)^-$, and $H_2C_4O_4$ have a large polarizability anisotropy (δ) of 53.6, 57.7, and 53.7, respectively, which are much larger than the value of $(CO_3)^{2-}$ that is 9.1. Therefore, these fundamental building units (FBUs) can induce large birefringence in crystals and are good functional modules for birefringent materials. The hyperpolarizability of the $(C_4O_4)^{2-}$ is zero owing to its centrosymmetric structure. As to $(HC_4O_4)^-$ and $H_2C_4O_4$, the existence of hydroxy group break the centrosymmetry of $(C_4O_4)^{2-}$ and results in large hyperpolarizability (β). The maximum absolute values of β tensor of $(HC_4O_4)^-$ and $H_2C_4O_4$ are 84.3 and −89.1, respectively, which are much larger than that of $(CO_3)^{2-}$ of 18.7. The above results reveal that the $(HC_4O_4)^-$ anionic group and the $H_2C_4O_4$ molecule are attractive FBUs to construct NLO materials.

Subsequently, $NaHC_4O_4{\cdot}H_2O$[30] is screened out by using the first-principles high-throughput screening pipeline for nonlinear optical materials (FPHS-NLO)[31] from the inorganic crystal structure database (ICSD). $NaHC_4O_4{\cdot}H_2O$ crystallizes in the noncentrosymmetric space group *Pc*. As shown in Figure 2, $(HC_4O_4)^-$ anions and H_2O molecules are hydrogen-bonded

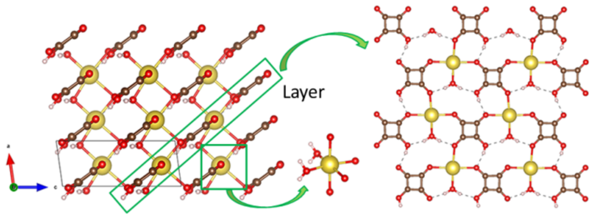

Figure 2. Crystal structure of $NaHC_4O_4{\cdot}H_2O$. The yellow, red, brown, and light pink balls represent Na, O, C, and H atoms, respectively.

to each other and form $[(HC_4O_4)^-{\cdot}H_2O]$ layers parallel to the *b* axis. Each Na atom is coordinated by two water molecules and four O atoms from different $(HC_4O_4)^-$ anions forming octahedra. Adjacent Na octahedra share their edges to form one-dimensional chains along the *a* axis. The chains cross and connect the $[(HC_4O_4)^-{\cdot}H_2O]$ layers to construct a stable three-dimensional network.

The single crystal of $NaHC_4O_4{\cdot}H_2O$ is prepared by a facile aqueous solution method (see experimental details in the Supporting Information). Finally, a rod-shaped crystal with a size of 30 × 6 × 5 mm was obtained (Figure 3a). The crystal structure was determined by single-crystal X-ray diffraction (XRD) analysis. The experimental details and crystal data are given in the Supporting Information. The purity of the crystal was confirmed by powder XRD (Figure 3b). The thermogravimetric (TG) and differential scanning calorimetry (DSC) curves indicates that $NaHC_4O_4{\cdot}H_2O$ is stable up to 418 K (Figure S1). The endothermal effect at 435 K on the DTA curve corresponds to a weight loss of 11.4% on the TG curve. This amount indicates the release of exactly one water molecule (11.7%) from the structure. The infrared (IR) spectra of $NaHC_4O_4{\cdot}H_2O$ are presented in Figure S2. The IR absorption peaks of 3507 and 3387 cm^{-1} represent a characteristic vibration of OH in crystal water molecules. The absorption bands at 1990 to 730 cm^{-1} confirm the existence of $(HC_4O_4)^-$ groups.[32]

The UV and IR transmittance spectrum are measured on an unpolished crystal with a thickness of about 1 mm. The result demonstrates that the UV cutoff edge of $NaHC_4O_4{\cdot}H_2O$ is about 350 nm, corresponding to an energy band gap of 3.54 eV (Figure 3c). The IR transmittance spectrum indicates the $NaHC_4O_4{\cdot}H_2O$ crystal is transparent up to 2.75 mm, covering the visible and near IR transparency band (Figure S3).

The SHG response of $NaHC_4O_4{\cdot}H_2O$ was measured by the Kurtz−Perry method under 1064 nm laser irradiation with the benchmark NLO crystal KDP used for reference. As shown in Figure 3d, the $NaHC_4O_4{\cdot}H_2O$ is type-I phase-matchable with a strong SHG efficiency of 2.3 × KDP. It is much larger than $(NH_4)_2C_2O_4{\cdot}H_2O$ (d_{14}(1.06 um) = 0.9 × d_{36}(KDP) = 0.31 pm/V).[28] To understand the relationship between the structure and optical properties, first-principles calculations are performed using the plane-wave DFT method by employing the CASTEP package.[33] The calculation details are given in the Supporting Information. As shown in Figure

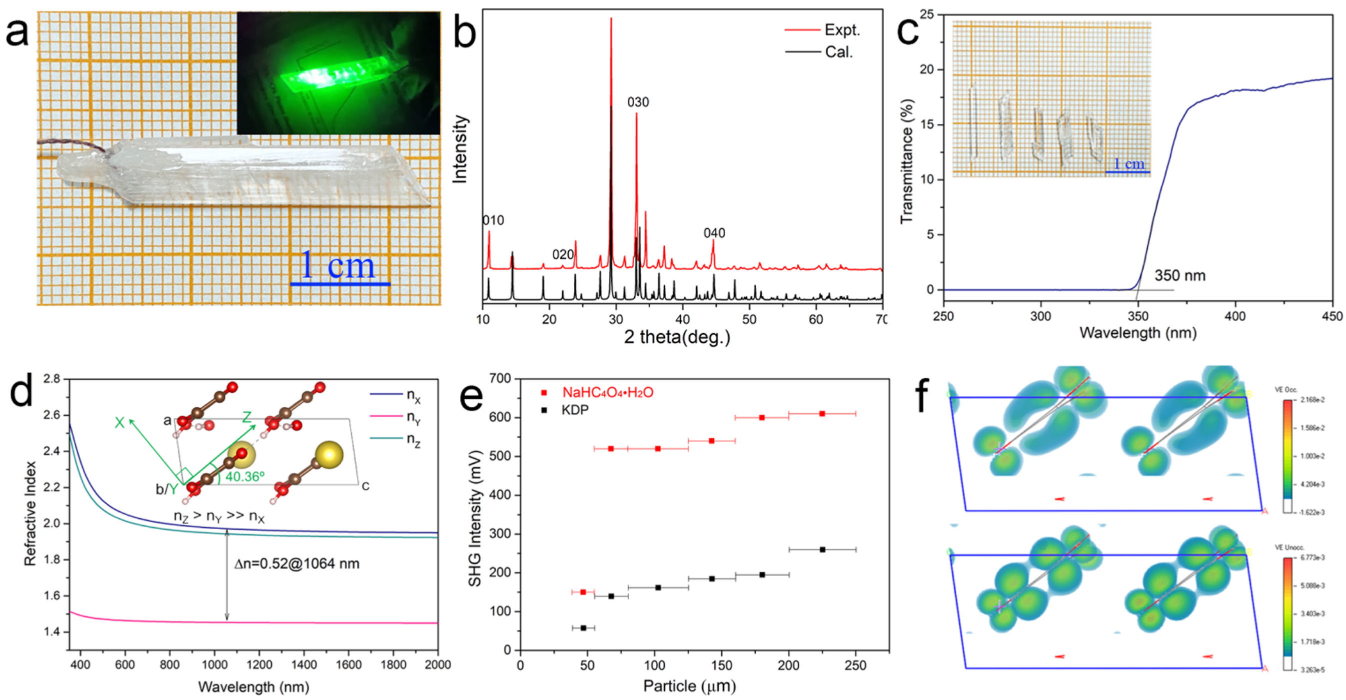

Figure 3. (a) Photograph of the $NaHC_4O_4{\cdot}H_2O$ crystal. (Inset: the crystal emits a bright green light under 1064 nm irradiation that indicates the generation of 532 nm light). (b) The experimental and calculated XRD patterns of $NaHC_4O_4{\cdot}H_2O$. The differences in peak intensity for the same crystallographic index between the experimental and calculated patterns are believed to be caused by the preferred orientation of the powder samples. It is in agreement with the needle-like shape of the title crystal. (c) UV transmission spectrum on single crystal of $NaHC_4O_4{\cdot}H_2O$. The inset presents the crystal plates. (d) Calculated refractive index and birefringence at 1064 nm. The inset shows the relationship between principle optical axes and the crystallographic axes. (e) Powder SHG measurements at 1064 nm. (f) SHG density map of the VE part of the largest SHG coefficient d_{33} of $NaHC_4O_4{\cdot}H_2O$.

S4, the calculated band structure indicates that $NaHC_4O_4{\cdot}H_2O$ has an indirect band gap of 2.68 eV. It is smaller than the experimental value of 3.54 eV because of the discontinuity of exchange−correlation energy functional.[34] The difference between them is corrected using a scissors operator when evaluating linear and nonlinear optical properties. $NaHC_4O_4{\cdot}H_2O$ belongs to the *m* point group and has six independent nonzero tensors. The calculated SHG coefficients are d_{11}= −1.09, d_{12}= −0.50, d_{13}= −1.69, d_{15}= −1.36, d_{24}= −0.69, and d_{33}= −2.11 pm/V. Considering the powder SHG intensity is a comprehensive reflection of all nonzero SHG tensors and related to point group and wavelength of incident laser. The calculated values are roughly agreement with the experimental one.

In order to identify the respective contribution of individual electronic states to SHG coefficients, the band-resolved method and SHG density method are adopted.[35] Figure 3f and Figure 4 display the SHG density map and the band-resolved virtual electron (VE) part of the largest SHG coefficient d_{33}. Combined with partial density of states (PDOS), one can find that the top of the valence bands and the bottom of the conduction bands give the vast majority of the contribution to d_{33} (Figure S5). In the valence bands, as shown in Figure 4, the third and fourth bands VB-3 and VB-4 make the dominant contribution. The orbital configurations of the two bands indicate they are constituted of delocalized π orbitals of four C atoms and anti-π orbitals of C═O (Figure S6). The highest two valence bands VB-1 and VB-2 that are constructed by C−C σ bonds and O nonbonding orbitals have no obvious contribution. This phenomenon is different from most NLO crystals in which the bands nearest the Fermi level give the most contribution to SHG coefficients.[36−41] In conduction bands, localized anti-π orbitals constructed by C and O atoms are the major contributor to the SHG coefficient. As shown in Figure 3f, these orbitals are highlighted in SHG density map. Overall, π orbitals of $(HC_4O_4)^-$ groups are the dominant source of SHG coefficient d_{33}. While Na and H_2O have no obvious contributions.

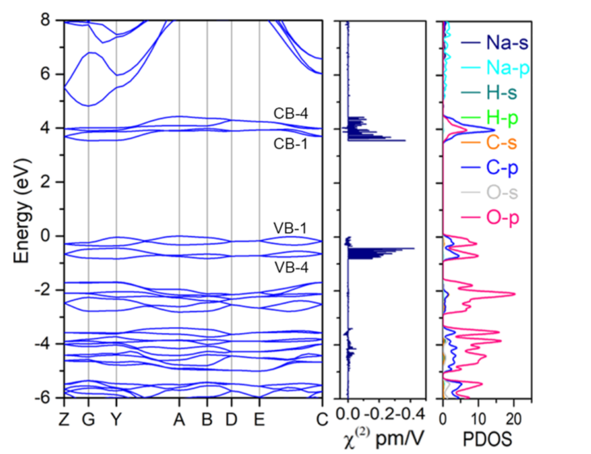

Figure 4. Band structure, partial density of states (PDOS), and band-resolved $\chi^{(2)}$ of $NaHC_4O_4{\cdot}H_2O$.

Birefringence is an important optical property. Birefringent materials can modulate the polarization of light and are critical for polarimetry, laser modulation, and optical communication. Besides, sufficient birefringence is the requirement for achieving phase-matching of NLO crystals. $NaHC_4O_4{\cdot}H_2O$ is

https://doi.org/10.1021/acsmaterialslett.2c00114
ACS Materials Lett. 2022, 4, 572−576

monoclinic and therefore an optically biaxial crystal. One of the principle optical axes is fixed to the crystallographic *b*-axis, and the other two principle optical axes are within the *ac*-plane. By diagonalizing static dielectric constant matrix obtained using the density-functional perturbation theory (DFPT) method, the relationships of the principle optical axes (*X*, *Y*, and *Z*) and crystallographic axes (*a*, *b*, and *c*) of $NaHC_4O_4 \cdot H_2O$ are determined (inset of Figure 3e). The refractive indices of $NaHC_4O_4 \cdot H_2O$ are calculated along optical axes. As shown in Figure 3e, $NaHC_4O_4 \cdot H_2O$ is a negative biaxial crystal with a relationship of refractive index of $n_Z > n_Y \gg n_X$. The birefringence is the difference between n_Z and n_X. $NaHC_4O_4 \cdot H_2O$ shows a giant birefringence at the transmittance window. The calculated birefringence at 1064 nm is 0.52 that is larger than the most widely used birefringent materials including $CaCO_3$ (0.171 @ 633 nm),[42] α-BaB_2O_4 (0.1222 @ 532 nm),[43] $Ca(BO_2)_2$,[44] and YVO_4 (0.225 @ 633 nm).[45] It is also much larger than the $(NH_4)_2C_2O_4 \cdot H_2O$ crystal (0.1587 at 546 nm).[27] One can find that the direction of the largest two refractive index n_Z and n_Y of the crystal lie in the $[(HC_4O_4)^- \cdot H_2O]$ layers, while the smallest refractive index n_X is perpendicular to the layers. The result is coincident with the calculated polarizability of the $(HC_4O_4)^-$ anionic group. Therefore, the large polarizability anisotropy and coplanar arrangement of $(HC_4O_4)^-$ groups result in a giant birefringence of the $NaHC_4O_4 \cdot H_2O$ crystal.

In summary, a π-conjugated planar hydrogensquarate $(HC_4O_4)^-$ with large hyperpolarizabilities and giant polarizability anisotropies is identified as a new NLO-active unit. The first squarates NLO crystal $NaHC_4O_4 \cdot H_2O$ was found by using FHSP-NLO. The crystal with size of 30 × 6 × 5 mm was grown by using aqueous solution method. $NaHC_4O_4 \cdot H_2O$ show a strong powder SHG effect of 2.3 × KDP and giant birefringence of 0.52 at 1064 nm. The results indicate that $NaHC_4O_4 \cdot H_2O$ would be a promising NLO and birefringent crystal. DFT calculation and analysis reveal that the $(HC_4O_4)^-$ group are the dominant source of SHG coefficient. This study provides a new promising NLO crystal and a novel NLO-active unit to design and synthesize NLO crystals.

ASSOCIATED CONTENT

Supporting Information

The Supporting Information is available free of charge at https://pubs.acs.org/doi/10.1021/acsmaterialslett.2c00114.

Crystal growth, crystal structure, thermogravimetric (TG), differential scanning calorimetry (DSC), infrared (IR) spectra, transmittance spectra, and DFT calculation results of $NaHC_4O_4 \cdot H_2O$ (PDF)

X-ray data (CIF)

AUTHOR INFORMATION

Corresponding Author

Bingbing Zhang − *College of Chemistry and Environmental Science, Hebei University, Baoding 071002, China;* orcid.org/0000-0002-1334-5812; Email: zhangbb@hbu.edu.cn

Authors

Xiaodong Zhang − *College of Chemistry and Environmental Science, Hebei University, Baoding 071002, China*

Dongxu Cao − *College of Chemistry and Environmental Science, Hebei University, Baoding 071002, China*

Daqing Yang − *College of Chemistry and Environmental Science, Hebei University, Baoding 071002, China;* orcid.org/0000-0002-3982-0263

Ying Wang − *College of Chemistry and Environmental Science, Hebei University, Baoding 071002, China;* orcid.org/0000-0001-6642-543X

Kui Wu − *College of Chemistry and Environmental Science, Hebei University, Baoding 071002, China;* orcid.org/0000-0001-8242-4613

Ming-Hsien Lee − *Department of Physics, Tamkang University, New Taipei City 25137, Taiwan;* orcid.org/0000-0003-3956-181X

Complete contact information is available at: https://pubs.acs.org/10.1021/acsmaterialslett.2c00114

Notes

The authors declare no competing financial interest.

ACKNOWLEDGMENTS

This work was supported by the National Natural Science Foundation of China (Grant Nos. 52072109, 21975062, and 51872324), the Natural Science Foundation of Hebei Province (Grant Nos. B2019201433 and E2019201049), and the Advanced Talents Incubation Program of the Hebei University (Grant No. 521000981279).

REFERENCES

(1) Tran, T. T.; Yu, H.; Rondinelli, J. M.; Poeppelmeier, K. R.; Halasyamani, P. S. Deep Ultraviolet Nonlinear Optical Materials. *Chem. Mater.* **2016**, *28* (15), 5238−5258.

(2) Mutailipu, M.; Yang, Z.; Pan, S. Toward the Enhancement of Critical Performance for Deep Ultraviolet Frequency-Doubling Crystals Utilizing Covalent Tetrahedra. *Acc. Mater. Res.* **2021**, *2* (4), 282−291.

(3) Wu, C.; Yang, G.; Humphrey, M. G.; Zhang, C. Recent Advances in Ultraviolet and Deep-Ultraviolet Second-Order Nonlinear Optical Crystals. *Coord. Chem. Rev.* **2018**, *375*, 459−488.

(4) Chen, X.; Jo, H.; Ok, K. M. Lead Mixed Oxyhalides Satisfying All Fundamental Requirements for High-Performance Mid-Infrared Nonlinear Optical Materials. *Angew. Chemie - Int. Ed.* **2020**, *59* (19), 7514−7520.

(5) Lan, H.; Liang, F.; Jiang, X.; Zhang, C.; Yu, H.; Lin, Z.; Zhang, H.; Wang, J.; Wu, Y. Pushing Nonlinear Optical Oxides into the Mid-Infrared Spectral Region Beyond 10 μm: Design, Synthesis, and Characterization of $La_3SnGa_5O_{14}$. *J. Am. Chem. Soc.* **2018**, *140* (13), 4684−4690.

(6) Mutailipu, M.; Yang, Z.; Pan, S. Toward the Enhancement of Critical Performance for Deep-Ultraviolet Frequency-Doubling Crystals Utilizing Covalent Tetrahedra. *Accounts Mater. Res.* **2021**, *2* (4), 282−291.

(7) Wu, Q.; Yang, C.; Liu, X.; Ma, J.; Liang, F.; Du, Y. Dimensionality Reduction Made High-Performance Mid-Infrared Nonlinear Halide Crystal. *Mater. Today Phys.* **2021**, *21*, 100569.

(8) Yang, C.; Liu, X.; Teng, C.; Cheng, X.; Liang, F.; Wu, Q. Hierarchical Molecular Design of High-Performance Infrared Nonlinear Ag_2HgI_4 Material by Defect Engineering Strategy. *Mater. Today Phys.* **2021**, *19*, 100432.

(9) Zhao, S.; Kang, L.; Shen, Y.; Wang, X.; Asghar, M. A.; Lin, Z.; Xu, Y.; Zeng, S.; Hong, M.; Luo, J. Designing a Beryllium-Free Deep-Ultraviolet Nonlinear Optical Material without a Structural Instability Problem. *J. Am. Chem. Soc.* **2016**, *138* (9), 2961−2964.

(10) Liu, X.; Kang, L.; Gong, P.; Lin, Z. $LiZn(OH)CO_3$: A Deep-Ultraviolet Nonlinear Optical Hydroxycarbonate Designed from a Diamond-like Structure. *Angew. Chemie - Int. Ed.* **2021**, *60* (24), 13574−13578.

(11) Zou, G.; Ye, N.; Huang, L.; Lin, X. Alkaline-Alkaline Earth Fluoride Carbonate Crystals $ABCO_3F$ (A = K, Rb, Cs; B = Ca, Sr, Ba) as Nonlinear Optical Materials. *J. Am. Chem. Soc.* **2011**, *133* (49), 20001−20007.

(12) Zhao, S.; Gong, P.; Bai, L.; Xu, X.; Zhang, S.; Sun, Z.; Lin, Z.; Hong, M.; Chen, C.; Luo, J. Beryllium-Free $Li_4Sr(BO_3)_2$ for Deep-Ultraviolet Nonlinear Optical Applications. *Nat. Commun.* **2014**, *5* (May), 4019.

(13) Boyd, G. D.; Miller, R. C.; Nassau, K.; Bond, W. L.; Savage, A. $LiNbO_3$: An Efficient Phase Matchable Nonlinear Optical Material. *Appl. Phys. Lett.* **1964**, *5* (11), 234−236.

(14) Xin, Y.; Mengkai, L.; Shaojun, Z.; Fuqi, L. Nonlinear Optical Properties of Perfectly Polarized KIO_3 Single Crystal. *Chin. Phys. Lett.* **1992**, *9* (2), 77−78.

(15) Chen, C.; Wang, Y.; Xia, Y.; Wu, B.; Tang, D.; Wu, K.; Wenrong, Z.; Yu, L.; Mei, L. New Development of Nonlinear Optical Crystals for the Ultraviolet Region with Molecular Engineering Approach. *J. Appl. Phys.* **1995**, *77* (6), 2268−2272.

(16) Chen, C.; Wu, Y.; Jiang, A.; Wu, B.; You, G.; Li, R.; Lin, S. New Nonlinear-Optical Crystal: LiB_3O_5. *J. Opt. Soc. Am. B* **1989**, *6* (4), 616−621.

(17) Chen, C.; Xu, Z.; Deng, D.; Zhang, J.; Wong, G. K. L.; Wu, B.; Ye, N.; Tang, D. The Vacuum Ultraviolet Phase-Matching Characteristics of Nonlinear Optical $KBe_2BO_3F_2$ Crystal. *Appl. Phys. Lett.* **1996**, *68* (21), 2930.

(18) Zhang, B.; Han, G.; Wang, Y.; Chen, X.; Yang, Z.; Pan, S. Expanding Frontiers of Ultraviolet Nonlinear Optical Materials with Fluorophosphates. *Chem. Mater.* **2018**, *30* (15), 5397−5403.

(19) Xiong, L.; Chen, J.; Lu, J.; Pan, C. Y.; Wu, L. M. Monofluorophosphates: A New Source of Deep-Ultraviolet Nonlinear Optical Materials. *Chem. Mater.* **2018**, *30* (21), 7823−7830.

(20) Liang, F.; Kang, L.; Zhang, X.; Lee, M. H.; Lin, Z.; Wu, Y. Molecular Construction Using $(C_3N_3O_3)^{3-}$Anions: Analysis and Prospect for Inorganic Metal Cyanurates Nonlinear Optical Materials. *Cryst. Growth Des.* **2017**, *17* (7), 4015−4020.

(21) Lin, D.; Luo, M.; Lin, C.; Xu, F.; Ye, N. $KLi(HC_3N_3O_3)\cdot 2H_2O$: Solvent-Drop Grinding Method toward the Hydro-Isocyanurate Nonlinear Optical Crystal. *J. Am. Chem. Soc.* **2019**, *141* (8), 3390−3394.

(22) Luo, M.; Lin, C.; Lin, D.; Ye, N. Rational Design of the Metal-Free $KBe_2BO_3F_2$ (KBBF) Family Member $C(NH_2)_3SO_3F$ with Ultraviolet Optical Nonlinearity. *Angew. Chemie - Int. Ed.* **2020**, *59* (37), 15978−15981.

(23) Wu, C.; Jiang, X.; Wang, Z.; Sha, H.; Lin, Z.; Huang, Z.; Long, X.; Humphrey, M. G.; Zhang, C. UV Solar-Blind-Region Phase-Matchable Optical Nonlinearity and Anisotropy in a π-Conjugated Cation-Containing Phosphate. *Angew. Chemie - Int. Ed.* **2021**, *60* (27), 14806−14810.

(24) Li, H.; Li, G.; Wu, K.; Zhang, B.; Yang, Z.; Pan, S. BaB_2S_4: An Efficient and Air-Stable Thioborate as Infrared Nonlinear Optical Material with High Laser Damage Threshold. *Chem. Mater.* **2018**, *30* (21), 7428−7432.

(25) Zhang, X.; Guo, L.; Zhang, B.; Yu, J.; Wang, Y.; Wu, K.; Wang, H.; Lee, M.-H. From Silicates to Oxonitridosilicates: Improving Optical Anisotropy for Phase-Matching as Ultraviolet Nonlinear Optical Materials. *Chem. Commun.* **2021**, *57* (5), 639−642.

(26) Tong, T.; Zhang, W.; Yang, Z.; Pan, S. Series of Crystals with Giant Optical Anisotropy: A Targeted Strategic Research. *Angew. Chemie Int. Ed.* **2021**, *60* (3), 1332−1338.

(27) Hobden, M. V. Phase-Matched Second-Harmonic Generation in Biaxial Crystals. *J. Appl. Phys.* **1967**, *38* (11), 4365−4372.

(28) Dmitriev, V. G.; Gurzadyan, G. G.; Nikogosyan, D. N. *Handbook of Nonlinear Optical Crystals*, 2nd ed.; Siegman, A. E., Ed.; Springer Series in Optical Sciences; Springer: Berlin, Heidelberg, 1997; Vol. *64*.

(29) Frisch, M. J., et al. *Gaussian09*, Revision D.01; Gaussian, Inc.: Wallingford, CT, 2009.

(30) Petrova, N.; Shivachev, B.; Kolev, T.; Petrova, R. Sodium Hydrogensquarate Monohydrate. *Acta Crystallogr E Struct Rep Online* **2006**, *E62* (6), m1359−m1361.

(31) Zhang, B.; Zhang, X.; Yu, J.; Wang, Y.; Wu, K.; Lee, M. H. First-Principles High-Throughput Screening Pipeline for Nonlinear Optical Materials: Application to Borates. *Chem. Mater.* **2020**, *32* (15), 6772−6779.

(32) Kolev, T.; Danchova, N.; Shandurkov, D.; Gutzov, S. Preparation and Spectral Properties of Europium Hydrogen Squarate Microcrystals. *Spectrochim. Acta - Part A Mol. Biomol. Spectrosc.* **2018**, *194*, 189−193.

(33) Clark, S. J.; Segall, M. D.; Pickard, C. J.; Hasnip, P. J.; Probert, M. I. J.; Refson, K.; Payne, M. C. First Principles Methods Using CASTEP. *Z. Kristallogr.* **2005**, *220* (5-6), 567−570.

(34) Wang, C. S.; Klein, B. M. First-Principles Electronic Structure of Si, Ge, GaP, GaAs, ZnS, and ZnSe. II. Optical Properties. *Phys. Rev. B* **1981**, *24* (6), 3417−3429.

(35) Lee, M.-H.; Yang, C.-H.; Jan, J.-H. Band-Resolved Analysis of Nonlinear Optical Properties of Crystalline and Molecular Materials. *Phys. Rev. B* **2004**, *70* (23), 235110.

(36) Li, S.; Liu, X.; Wu, H.; Song, Z.; Yu, H.; Lin, Z.; Hu, Z.; Wang, J.; Wu, Y. $Ba_4Ca(B_2O_5)_2F_2$: π-Conjugation of B_2O_5 in the Planar Pentagonal Layer Achieving Large Second Harmonic Generation of Pyro-Borate. *Chem. Sci.* **2021**, 2−6.

(37) Yan, H.; Matsushita, Y.; Yamaura, K.; Tsujimoto, Y. $La_3Ga_3Ge_2S_3O_{10}$: An Ultraviolet Nonlinear Optical Oxysulfide Designed by Anion-Directed Band Gap Engineering. *Angew. Chemie Int. Ed.* **2021**.*133*2676*5*

(38) Li, Z.; Jin, W.; Zhang, F.; Chen, Z.; Yang, Z.; Pan, S. Achieving Short-Wavelength Phase-Matching Second Harmonic Generation in Boron-Rich Borosulfate with Planar $[BO_3]$ Units. *Angew. Chemie Int. Ed.* **2022**.*61*e202112844

(39) Zhang, B.; Yang, Z.; Yang, Y.; Lee, M.-H.; Pan, S.; Jing, Q.; Su, X. P-(p,π*) Interaction Mechanism Revealing and Accordingly Designed New Member in Deep-Ultraviolet NLO Borates $Li_nM_{n-1}B_{2n-1}O_{4n-2}$ (M = Cs/Rb, n = 3, 4, 6). *J. Mater. Chem. C* **2014**, *2* (21), 4133−4141.

(40) Qi, L.; Chen, Z.; Shi, X.; Zhang, X.; Jing, Q.; Li, N.; Jiang, Z.; Zhang, B.; Lee, M.-H. $A_3BBi(P_2O_7)_2$ (A = Rb, Cs; B = Pb, Ba): Isovalent Cation Substitution to Sustain Large Second-Harmonic Generation Responses. *Chem. Mater.* **2020**, *32* (19), 8713−8723.

(41) Lu, X.; Chen, Z.; Shi, X.; Jing, Q.; Lee, M. Two Pyrophosphates with Large Birefringences and Second-Harmonic Responses as Ultraviolet Nonlinear Optical Materials. *Angew. Chemie Int. Ed.* **2020**, *59* (40), 17648−17656.

(42) Ghosh, G. Dispersion-Equation Coefficients for the Refractive Index and Birefringence of Calcite and Quartz Crystals. *Opt. Commun.* **1999**, *163* (1), 95−102.

(43) Appel, R.; Dyer, C. D.; Lockwood, J. N. Design of a Broadband UV-Visible α-Barium Borate Polarizer. *Appl. Opt.* **2002**, *41* (13), 2470.

(44) Chen, X.; Zhang, B.; Zhang, F.; Wang, Y.; Zhang, M.; Yang, Z.; Poeppelmeier, K. R.; Pan, S. Designing an Excellent Deep-Ultraviolet Birefringent Material for Light Polarization. *J. Am. Chem. Soc.* **2018**, *140* (47), 16311−16319.

(45) DeShazer, L. G. Improved Midinfrared Polarizers Using Yttrium Vanadate. *Proc. SPIE* **2001**, *4481*, 10−16.

https://doi.org/10.1021/acsmaterialslett.2c00114
ACS Materials Lett. 2022, 4, 572−576